High Modulus Polypropylene Fibers. II. Influence of Fiber Preparation upon Structure and Morphology

Diana Gregor-Svetec

Department of Textiles, Faculty of Natural Sciences and Engineering, University of Ljubljana, SI-1000 Ljubljana, Slovenia

Received 23 November 2004; accepted 13 June 2005
DOI 10.1002/app.23415
Published online in Wiley InterScience (www.interscience.wiley.com).

ABSTRACT: The influence of drawing on the limiting draw ratio upon formation of the morphological structure of fibers spun from binary polypropylene (PP) blends was studied. Fibers were spun from a fiber-grade CR-polymer and from the blends of a fiber-grade CR-polymer with a molding-grade polymer in the composition range of 10–50 wt % added. As-spun fibers were immediately moderately and additionally highly drawn at the temperature of 145°C. The structure and morphology of these fibers were investigated by small-angle X-ray scattering, wide-angle X-ray scattering, differential scanning calorimetry, scanning electron microscopy, density, birefringence, and sound velocity measurements. It was shown that continuously moderately drawn fibers are suitable precursors for the production of high tenacity PP fibers of very high modulus, because of so called oriented "smectic" structure present in these fibers. With drawing at elevated temperature, the initial metastable structure of low crystallinity was disrupted and a *c*-axis orientation of monoclinic crystalline modification was developed. Hot drawing increased the size of crystallites and crystallinity degree, the orientation of crystalline domains, and average orientation of the macromolecular chains and resulted in extensive fibrillation and void formation. It was found that the blend composition has some influence on the structure of discontinuously highly drawn fibers. With increasing the content of the molding-grade polymer in the blend, the size of crystalline and amorphous domains, density and crystallinity, as well as amorphous orientation decreased. Relationship has been established between the mechanical properties, crystallinity, and orientation of PP fibers. It was confirmed that by blending the fiber-grade CR-polymer by a small percentage of the molding-grade polymer, maximization of elastic modulus is achieved, mainly because of higher orientation of amorphous domains. © 2006 Wiley Periodicals, Inc. J Appl Polym Sci 100: 1067–1082, 2006

Key words: polypropylene (PP); SAXS; WAXS; structure-property relations

INTRODUCTION

With polypropylene (PP), as with all man-made fibers, there is a continuing search for means of producing fibers with improved properties. Improved properties with respect to the tenacity and modulus are only one of the many possibilities of PP-engineering to obtain new special fibers with a high added value intended for special purposes. Our previous work, presented in Part 1 of this paper, showed that the PP fibers of high moduli (an elastic modulus up to 14.8 GPa and dynamic modulus up to 19 GPa) could be produced by melt spinning followed by more-stage drawing process, using industrially feasible conditions. A suitable polymer and processing conditions for the production of the high modulus PP fibers have been identified.[1] In this study, a more detailed investigation of the structure and the relationship between the structural parameters and mechanical properties are presented.

In common with the other synthetic fibers, the mechanical properties of PP fibers are strongly influenced by their physical structure, which is controlled by both the choice of the starting material and the fiber formation conditions. The different conditions of the fiber formation during the melt spinning and drawing cause different arrangements of the supermolecular structural elements, which result in different fiber properties.[2–7] The structure and final properties of fibers also depend on their molecular structure, i.e., polymer molecular mass and molecular mass distribution.[8–15] The morphological changes occurring in the semicrystalline polymers as a result of drawing have been extensively investigated. Varying views of structural and property changes resulting from drawing have been expressed by Peterlin and Samuels. Samuels[16,17] investigated the variation in orientation and morphology during drawing; mechanical properties of drawn fibers were measured and correlated with orientation. Peterlin's attempt to interpret morphology variations during the drawing of PE and PP

Correspondence to: D. Gregor-Svetec (diana.gregor@ntf.uni-lj.si).

Contract grant sponsors: Ministry of Research and Technology, Slovenia, University of Graz.

resulted in a widely accepted microfibrillar structural model.[18,19] Another structural model was developed by Taylor and Clark to interpret the structure of highly drawn polymers.[20] The structure formation in PP fibers was recently presented by Spruiell[21] and by Koike and Cakmak,[22] whereas Hautojärvi and Niemi,[23] Broda,[24] and Risnes et al.[25] studied the morphology of PP fibers.

EXPERIMENTAL

Preparation of PP fibers

Fibers were spun from a blend of two commercial PP chips, Hostalen PPU 1780F2, a fiber-grade CR-polymer with MFR = 18 g/10 min and Hostalen PPN 1060F, a molding-grade homopolymer with MFR = 2 g/10 min. Blends composed of 90/10, 80/20, 70/30, and 50/50 fiber/molding-grade polymer by weight were prepared. From these polymer blends and from the pure fiber-grade CR-polymer, fibers were produced by melt spinning. The melt spinning and continuous three-stage drawing of PP at 50°C fibers was carried out on a laboratory spin-draw device (Extrusion Systems Ltd., Bradford, UK). These fibers of series I are herein indicated as continuously drawn fibers. In the subsequent drawing process on a laboratory draw device (Zimmer AG, Frankfurt, Germany), the continuously moderately drawn fibers were additionally drawn at 145°C to the limiting draw ratio. These fibers of series II are herein indicated as discontinuously drawn fibers. Further processing details were reported previously in Part 1 of this paper.[26]

Techniques

Wide-angle X-ray scattering (WAXS) and small-angle X-ray scattering (SAXS) techniques were used to explore the structure of drawn PP fibers. A copper radiation was monochromatized by means of a 10-μm Ni filter. WAXS and SAXS film patterns were taken on a vacuum flat-film camera with pinhole collimation. WAXS curves (intensity as a function of scattering angle (2θ)) were plotted for normal transmission geometry of samples by using a two-circle goniometer developed by Kratky. The scattered intensities were registered with a position-sensitive detector Braun PSD 50M, in the angular range from $2\theta = 9.5°$ to 31.5° for each azimuthal position of the fiber axis from $\phi = 0°$ to 180°. The intensities obtained were corrected for polarization, absorption, background, and incoherent scattering. The degree of crystallinity was estimated by the Hermans and Weidinger method[27] over the angular range from $2\theta = 10°$ to 30°. The apparent crystallite dimensions were determined by means of the Scherrer's equation.[28] The crystalline orientation function was calculated with the help of (110) and (040) reflections, using the Wilchinsky[29] relation for a monoclinic crystal system.

SAXS curves were obtained by using a Kratky block camera with slit collimation. Scattered intensities were registered with a conventional proportional detector. The long period was determined from the meridional SAXS reflection via the calculated one-dimensional intensity function. The observed scattering function was approximated with a model function, on the basis of a stacking model as described by Brämer.[30,31] From diffuse SAXS, the volume fraction of voids present in solid polymers was estimated. SAXS curves were evaluated in accordance with the Porod's theory, by assuming a dense two-phase system (polymer/voids).[32,33]

Morphological studies involved scanning electron microscopy of the filament surface and inner structure. Several samples were split to expose the inner structure. Filaments were also etched in a chromic acid solution at room temperature. A JEOL JSM-2 electron microscope was used for all morphological studies. The magnification obtained is indicated by a 10-μm bar on the micrographs.

The crystalline fraction in fibers was evaluated also from density data and differential scanning calorimetry (DSC) thermograms. The density of drawn fibers was determined with the flotation method as described by Juilfs,[34] using a mixture of isopropylalcohol and water. The melting behavior of the samples in the temperature range from 40 to 200°C was examined at a constant heating rate of 10°C/min with a Perkin-Elmer DSC-7 calorimeter.

The birefringence of the filaments was measured using a polarizing light microscope and an Ehringhaus compensator. The degree of molecular orientation was estimated from the birefringence using an equation proposed by Stein.[35] The average molecular orientation was obtained by the sonic-velocity method. The velocity of sound waves in the filaments was measured on a Morgan's Dynamic Modulus Tester PPM-5R. The amorphous orientation function was calculated in a manner applied to PP by Samuels.[36]

RESULTS AND DISCUSSION

Polymorphism

Depending on the crystallization conditions, PP chains of 3_1 helical conformation can be organized into different spatial arrangements giving rise to three crystalline modifications: α-monoclinic, β-hexagonal, γ-orthorombic, and one mesomorfic, the so-called "smectic" form. Among all these crystal structures, the α-monoclinic form is the most thermodynamically stable one and therefore the most common. On WAXS diffraction curves (intensity as a function of scattering angle (2θ)) of drawn fibers shown in Figures 2 and 4,

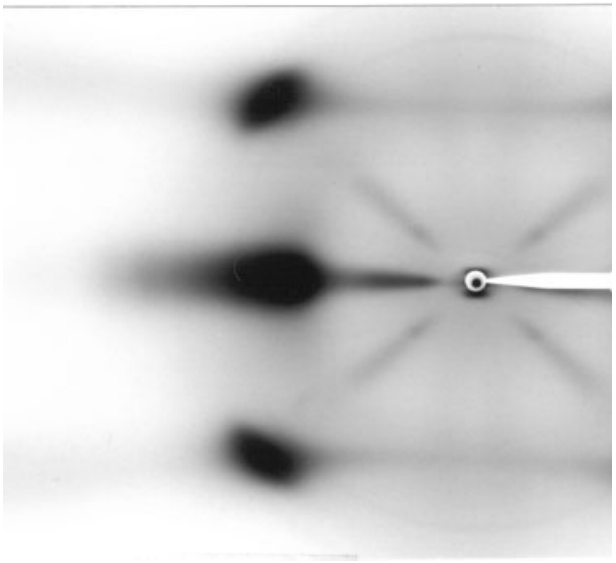

Figure 1 WAXS film pattern (fiber axis vertical) of continuously drawn fiber, spun from the 100/0 fiber/molding grade polymer blend.

a different crystal structure can be seen. Continuously drawn fibers show wide and diffuse equatorial spots of the (110), (040), and (130) planes united in one reflection on the WAXS film pattern (Fig. 1). Overlapping of (110), (040), and (130) equatorial peaks is also seen on WAXS diffraction patterns (Fig. 2). This equatorial maximum at $2\theta = 14.6°$ and a second broad peak at $2\theta = 21.2°$ indicate the presence of the so-called oriented smectic structure, first discussed by Natta and Corradini.[37] They categorized it as a smectic structure with an intermediate degree of ordering between the amorphous and crystalline phases. Other investigators described this partially ordered domain, where the individual chains maintain the threefold helical conformation and the parallel arrangement along the fiber axis, as paracrystalline,[38] composed of microcrystallites[39–43] or nanocrystallites,[44] or as a form that consists of clusters of ordered helical chain segments with a random assembly of helical hands.[45] The overlapping of equatorial reflections is the consequence of the broadening effect of very small or very imperfect crystallites. The small value of around 3.5 nm of the lateral crystallite dimensions, as determined from the half-width of the equatorial peak, confirms the presence of small crystallites. Even if we were able to separate all three united equatorial reflections, their intensities would be small, the values of half-width of peaks would be large, and so, the crystallite size would remain small. This implies that crystal size broadening may be considered to be responsible for the typical WAXS pattern, as also interpreted by Bodor et al.[41]

All discontinuously drawn fibers have a discrete pattern, typical for a crystalline and oriented system, seen on the WAXS film pattern of fiber spun from the 100/0 fiber/molding-grade polymer blend (Fig. 3). The strong reflection peaks can be found at the scattering angles 2θ of 14° (110), 17° (040), 18.5° (130), 21° (111), and 22° ($\bar{1}$ 31) and 041)), indicating the presence of α-monoclinic crystal structure. This typical pattern of a well-oriented fibrous structure, with the above broad equatorial maximum split up into narrower (110), (040), and (130) reflections, is clearly seen on the WAXS curves too (Fig. 4). Only *c*-axis orientation of monoclinic crystallites is present in these fibers.

Nanostructure from WAXS and SAXS

X-ray diffraction curves of the crystalline peaks were approximated by pseudo-Voigt functions and the apparent crystallite dimensions were determined from the half-width reflections by applying Sherrer's equation:

$$D_{\mathrm{hkl}} = \frac{\lambda K}{\beta \cos\theta} \tag{1}$$

where D_{hkl} represents the apparent crystallite size, λ the wavelength used, β the width of half-maximum intensity of the reflection profile corrected for instrumental broadening, θ the diffraction angle, and K is a constant that is commonly assigned a value of 0.9 for PP. From the equatorial reflections, the size of crystallites in directions [110], [010], and [130], i.e., perpendicular to the fiber axis could be obtained. Because of the absence of the meridional reflection, the dimension of crystallites in the direction of fiber axis could not be determined in the same way. The size of crystallite was calculated from the following equation:

$$D_c = \frac{L x_c \rho}{\rho_c} \tag{2}$$

where L is long period, ρ density and x_c degree of crystallinity of the sample, and ρ_c the density of a perfect polymer crystal. The dimensions of ordered—crystalline and less ordered—amorphous domains are shown in Figure 5. The apparent crystallite size, as well as the size of the amorphous part, for continuously drawn fiber is low. With the additional hot drawing, the size of crystallites increased in both directions: perpendicular and along the fiber axis. At the discontinuously drawn fibers also, the size of amorphous domain is larger in comparison with the amorphous domain of continuously drawn fibers. As seen from Figure 5, the dimensions of crystalline and amorphous domains of the continuously drawn fibers do not change, whatever the blend composition. For dis-

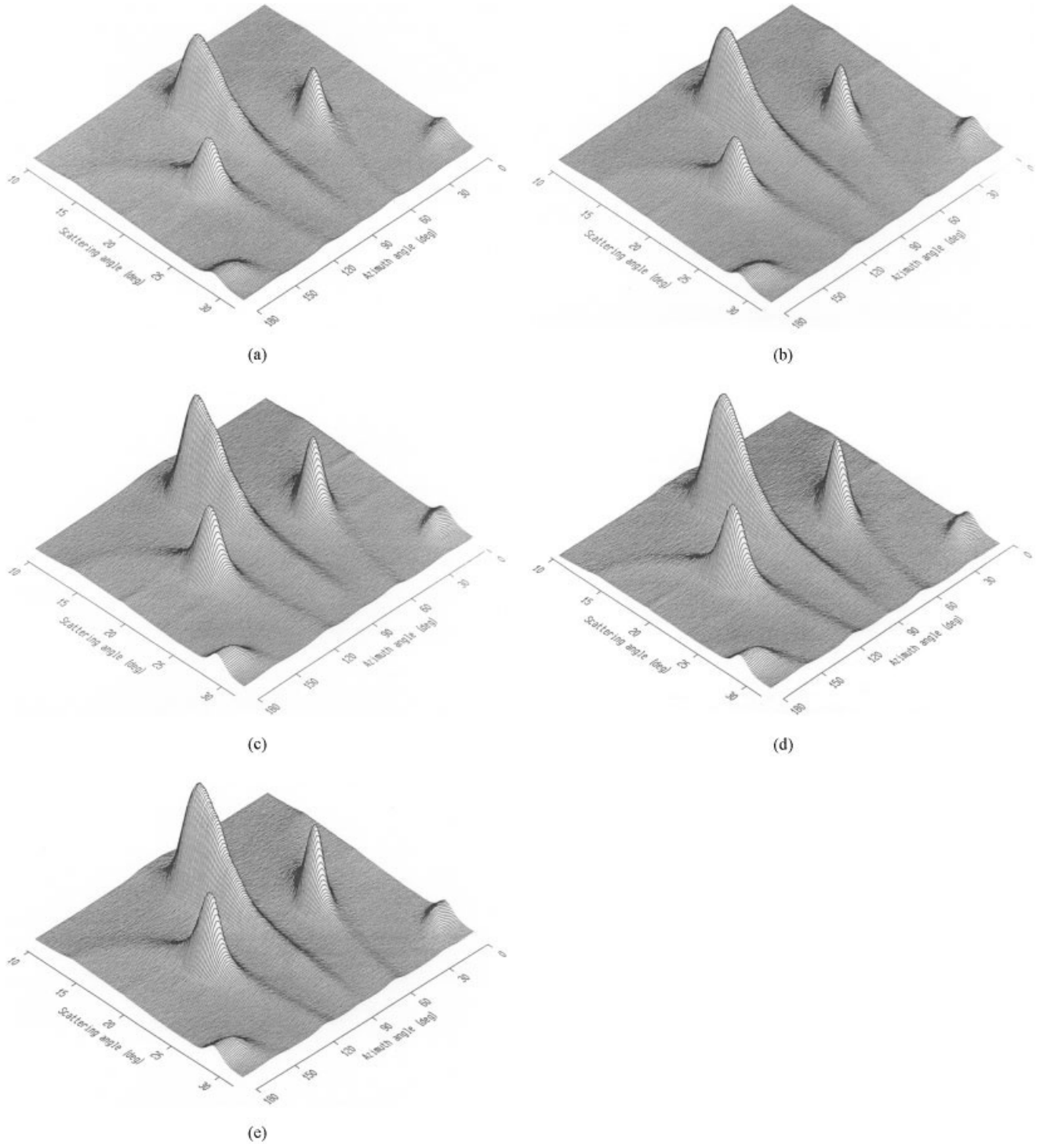

Figure 2 WAXS diffraction curves of continuously drawn fibers, spun from the (a) 100/0 fiber/molding grade polymer blend, (b) 90/10 fiber/molding grade polymer blend, (c) 80/20 fiber/molding grade polymer blend, (d) 70/30 fiber/molding grade polymer blend, and (e) 50/50 fiber/molding grade polymer blend.

continuously drawn fibers, no change with the blend composition is seen for the size of crystallites perpendicular to the fiber axis, while the dimensions of domains in the direction of fiber axis are not the same. With the addition of the molding-grade polymer to the fiber-grade CR-polymer, the draw ratio is lowered, and with it, the size of the crystalline and amorphous domains are also lowered. A slight increase in the size of crystallites and even higher increase in the size of amorphous domain is seen only at the discontinuously drawn fiber, spun from the 90/10 fiber/molding-grade polymer blend composition.

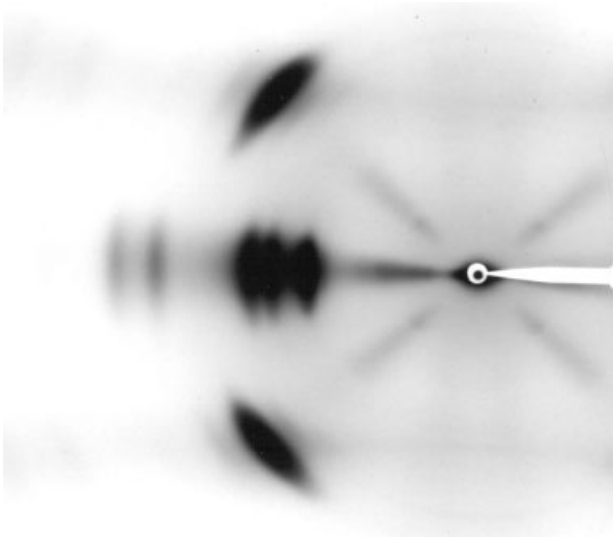

Figure 3 WAXS film pattern (fiber axis vertical) of discontinuously drawn fiber, spun from the 100/0 fiber/molding grade polymer blend.

Degree of crystallinity

Different analytical methods were used for the determination of the degree of crystallinity. The crystallinity index was evaluated from the WAXS diffraction curves over the angular range from $2\theta = 10°–30°$ by resolving multiple peak data into individual crystalline peaks and an amorphous halo. In accordance with Hermans-Weidinger's definition, the crystallinity was calculated as the ratio of the integrated scattering under the resolved crystalline peaks to the total scattering of the sample. A mass crystallinity index was calculated as a percentage based on measured densities using following relation

$$x_{c,\text{density}} = \frac{\rho_c(\rho - \rho_{\text{am}})}{\rho(\rho_c - \rho_{\text{am}})} \times 100\ (\%) \qquad (3)$$

where ρ represents the density of sample, ρ_c the density of a perfect polymer crystal (0.938 g/cm^3), and ρ_{am} the density of an amorphous polymer (0.8545 g/cm^3). By the DSC method, the crystallinity index was derived as a ratio of the measured heat of fusion to the heat of fusion of 100% crystalline polymer, with a value of 206 J/g.

Crystallinity values obtained from the X-ray data, density measurements, and DSC method as a function of the blend composition are presented in Figure 6. As seen from Figure 6, the blend composition has some influence on the crystallinity index. At the continuously drawn fibers an increase up to 5% for values obtained from WAXS data and upto 10% for values obtained from density measurements was noted with increasing the content of the molding-grade polymer in the blend. The same tendency is seen with the discontinuously drawn fibers, where crystallinity evaluated from the WAXS curves increases up to 70/30 fiber/molding-grade polymer blend and then at 50/50 fiber/molding-grade polymer blend drops to a value of 41.8%, which is the lowest crystallinity index determined by this method at highly drawn fibers. Quite different results were obtained by other two methods, where with increasing the content of the molding-grade polymer in the blend, lower values of crystallinity were obtained. It is interesting to observe from these results that the crystallinity values determined from the density measurements at discontinuously drawn fibers are as low as or even lower than that of the continuously drawn fibers. Lower values of crystallinity determined by the density method in comparison with values obtained by other two methods have been attributed to increased levels of fibrillation and void formation during drawing to the limiting draw ratio. The formation of microvoids throughout the polymer matrix reduces the crystallinity derived from density measurements and leaves the crystallinity derived from DSC measurements unaffected, since the heat of fusion is mass-based. The difference in absolute values between the crystallinity derived from WAXS and DSC methods is the consequence of evaluation of the WAXS data. Here we assume that the structure of fibers consists of two parts, an oriented—the crystalline and an isotropic—amorphous part. The oriented contribution is from all oriented fraction of the material, while the unoriented scattering, which is subtracted from the oriented one, contains the contribution of scattering of the amorphous chains and from the isotropically oriented crystals, and therefore, these crystals are not included in the crystallinity index.

Long period and microvoids

A Typical SAXS film pattern of continuously drawn fibers and discontinuously drawn fibers, together with the measured SAXS curve approximated with the calculated model function, is shown in Figures 7 and 8, respectively. The continuously drawn fibers exhibit a two-point pattern with weak intensity maxima on the meridian and a weak diffuse equatorial scattering (Fig. 7(a)), which indicates the presence of microvoids. At continuously drawn fibers, the location of the peak and the intensity of the peak are the same for all fibers, spun from different blend compositions. The peak position is located at about 0.55 nm, which corresponds to a long period of about 11.4 nm. As seen on the SAXS film pattern of discontinuously drawn fiber, no meridional small angle reflection appears (Fig. 8(a)). The absence of the meridional reflection could be explained by dissolution of lamellar structure, assuming that the regular alternation of crystalline and amorphous regions is disrupted on drawing by exten-

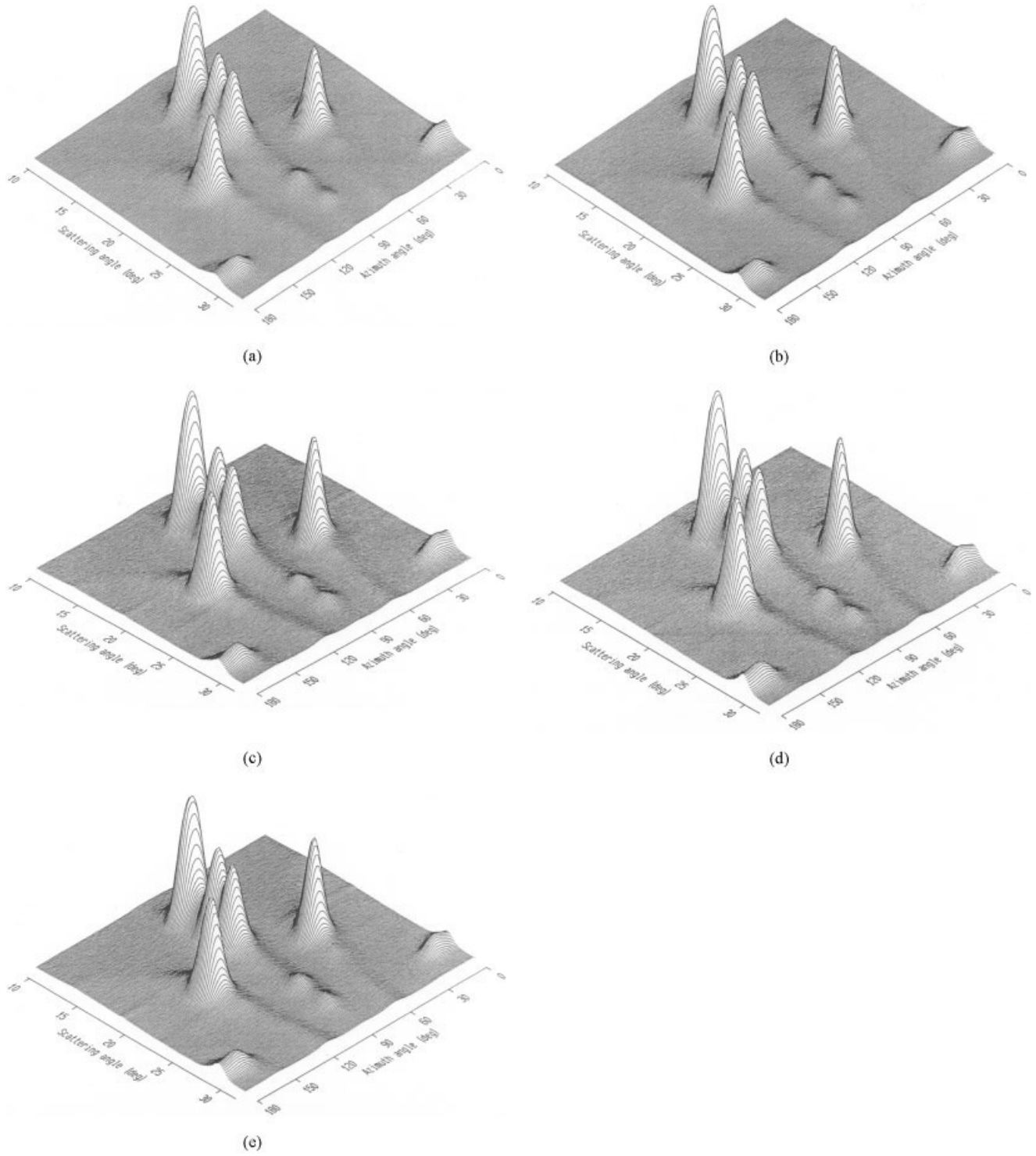

Figure 4 WAXS diffraction curves of discontinuously drawn fibers, spun from the (a) 100/0 fiber/molding grade polymer blend, (b) 90/10 fiber/molding grade polymer blend, (c) 80/20 fiber/molding grade polymer blend, (d) 70/30 fiber/molding grade polymer blend, and (e) 50/50 fiber/molding grade polymer blend.

sion of the molecular chains and subsequent formation of voids. These crystalline and amorphous regions are now irregularly rearranged in adjacent microfibrils. As a result there is a lack of sufficient scattering power, the difference in electron density decreases considerably, which diminishes the intensity of the meridional reflection. At the same time, very strong diffuse equatorial scattering appears, due to inhomogenities in electron distribution. A strong equatorial streak represents the fibrillar morphology

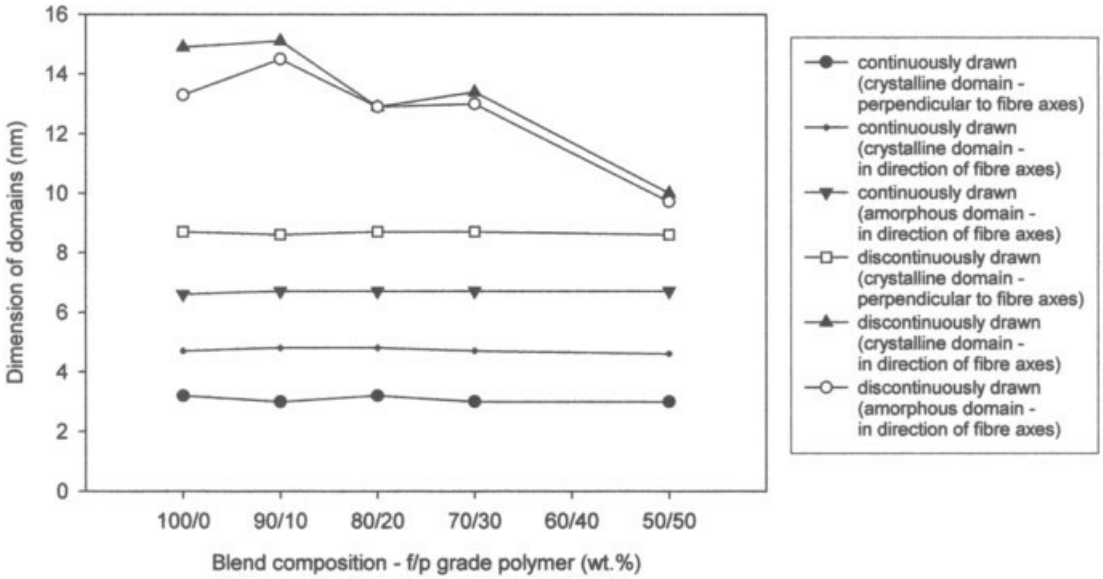

Figure 5 The dimensions of crystalline and amorphous domains, i.e., the apparent size of crystallites perpendicular to fiber axis and in direction of fiber axis of continuously and discontinuously drawn fibers, spun from the 100/0, 90/10, 80/20, 70/30, and 50/50 fiber/molding grade polymer blend.

and the typical "diamond" shaped pattern indicates the presence of large voids elongated parallel to the filament axis. Because of the absence of a maximum in the meridian, the long period at discontinuously drawn fibers could not be determined from Bragg's equation as for the continuously drawn fibers. Values for the long period were obtained from the constructed model function on the basis of a stacking model as described by Brämer (Fig. 8(b)) and can be taken as approximately predicted values. It was established that with additional hot drawing the long period, i.e., the distance between the centers of two adjacent crystalline domains along fiber axis, increased more than two times. Values between 21.4 and 29.6 nm were obtained, the highest being at fiber spun from the 90/10 fiber/molding-grade polymer blend.

To obtain information about the concentration of the microvoids, the volume fraction of microvoids was

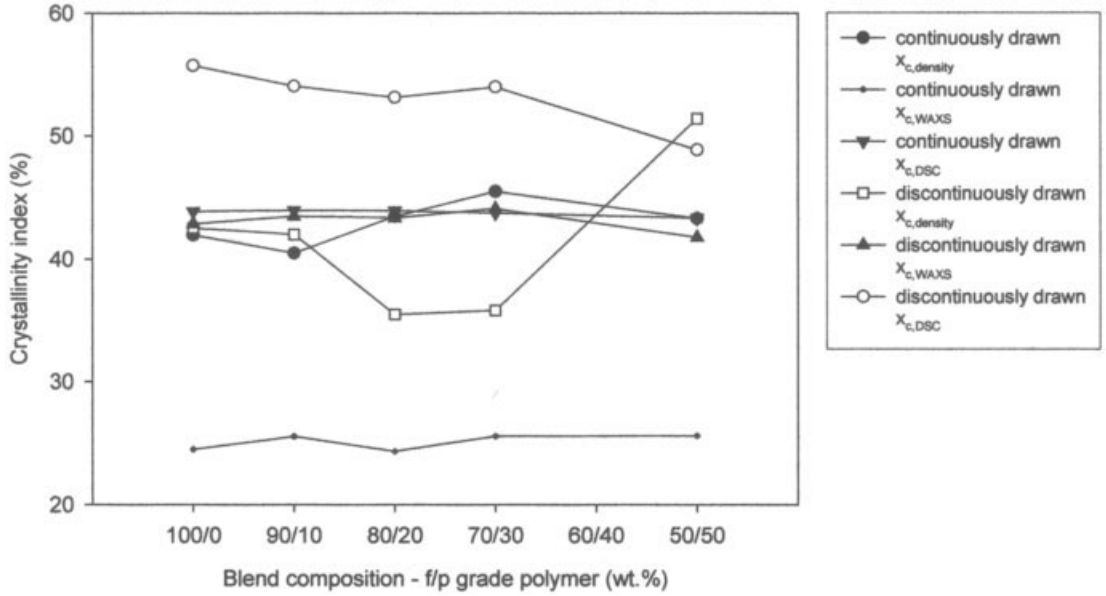

Figure 6 Degree of crystallinity evaluated from WAXS curves ($x_{c,\mathrm{WAXS}}$), DSC-themograms ($x_{c,\mathrm{DSC}}$) and density data ($x_{c,\mathrm{density}}$) of continuously and discontinuously drawn fibers, spun from the 100/0, 90/10, 80/20, 70/30, and 50/50 fiber/molding grade polymer blend.

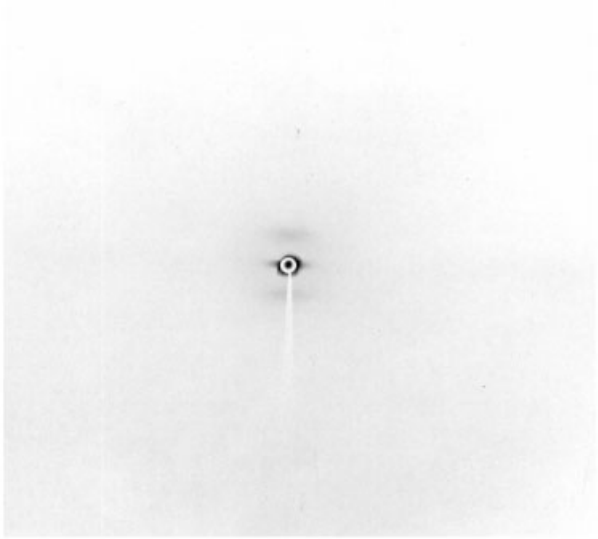

(a)

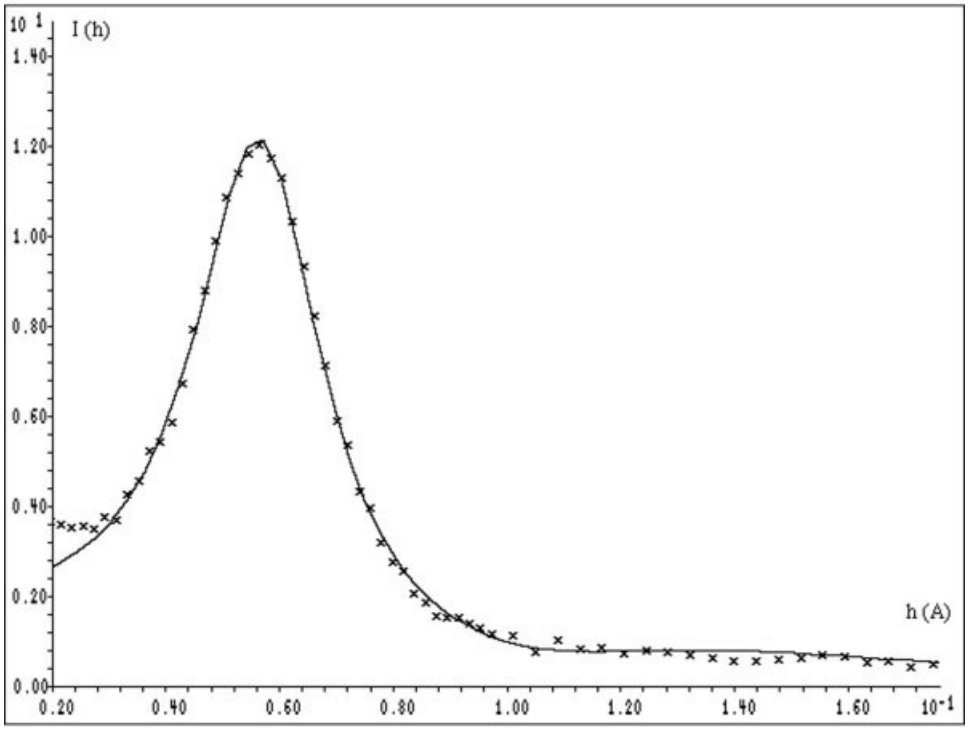

(b)

Figure 7 (a) SAXS film pattern (fiber axis vertical) and (b) measured SAXS curve of continuously drawn fiber, spun from the 100/0 fiber/molding grade polymer blend, approximated with the model function.

determined from SAXS curves. For the continuously drawn fibers, a volume fraction between 1.2 and 1.8% was obtained, which is in the range of reported values for drawn polymers. Much higher values of microvoid content were obtained for the discontinuously drawn fibers, ranging from 4% for fiber spun from 50/50 fiber/molding-grade polymer blend to 9.6% for fiber spun from the 90/10 fiber/molding-grade polymer blend.

Morphology from SEM

Electron microscopy was used to examine in some detail the morphological changes that occurred on drawing. In Figures 9 and 10, surface features of moderately and highly drawn fibers are shown. The continuously drawn fibers remained transparent after drawing. Under the microscope fibers exhibited smooth surface, without any surface features (Fig.

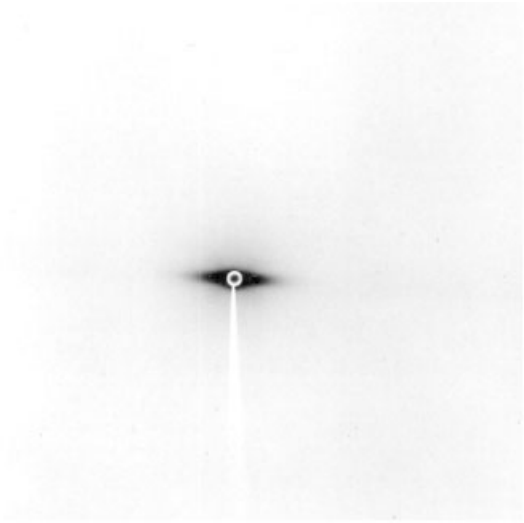

(a)

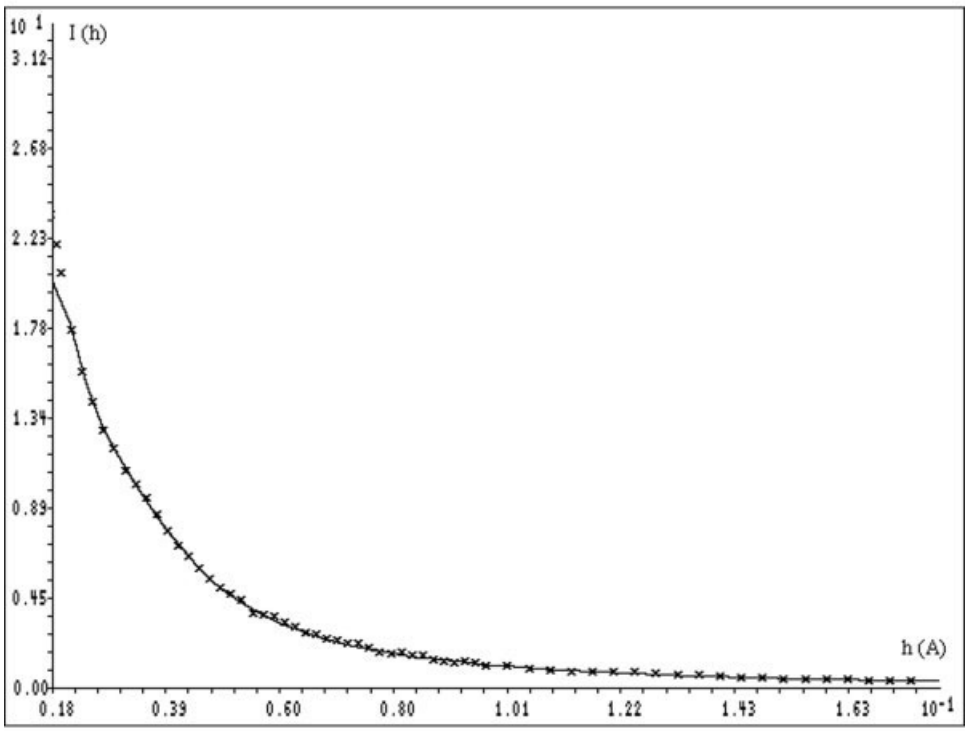

(b)

Figure 8 (a) SAXS film pattern (fiber axis vertical) and (b) measured SAXS curve of discontinuously drawn fiber, spun from the 100/0 fiber/molding grade polymer blend, approximated with the model function.

9(a)). Additional hot drawing has drastically changed the appearance of fibers. Discontinuously drawn fibers became visibly opaque and cloudy after drawing. This "whitening" phenomenon indicates the presence of a great many voids with magnitude of the order of optical wavelength. Investigation of the surface by electron microscopy revealed craze-like markings perpendicular to the fiber axis (Fig. 10(a)). A craze can be defined as a zone spanned by aligned fibrils alternating with elongated voids both being parallel to the draw direction.[46] These planes correspond to the strain-induced "transverse lines" observed by optical microscopy (Fig. 11). Examination of the internal texture by splitting and etching indicated that morphological changes were not restricted only to the surface layers. While continuously drawn fibers could not be split without extensive plastic deformation (Fig. 9(b)), discontinuously drawn fibers could be split, because

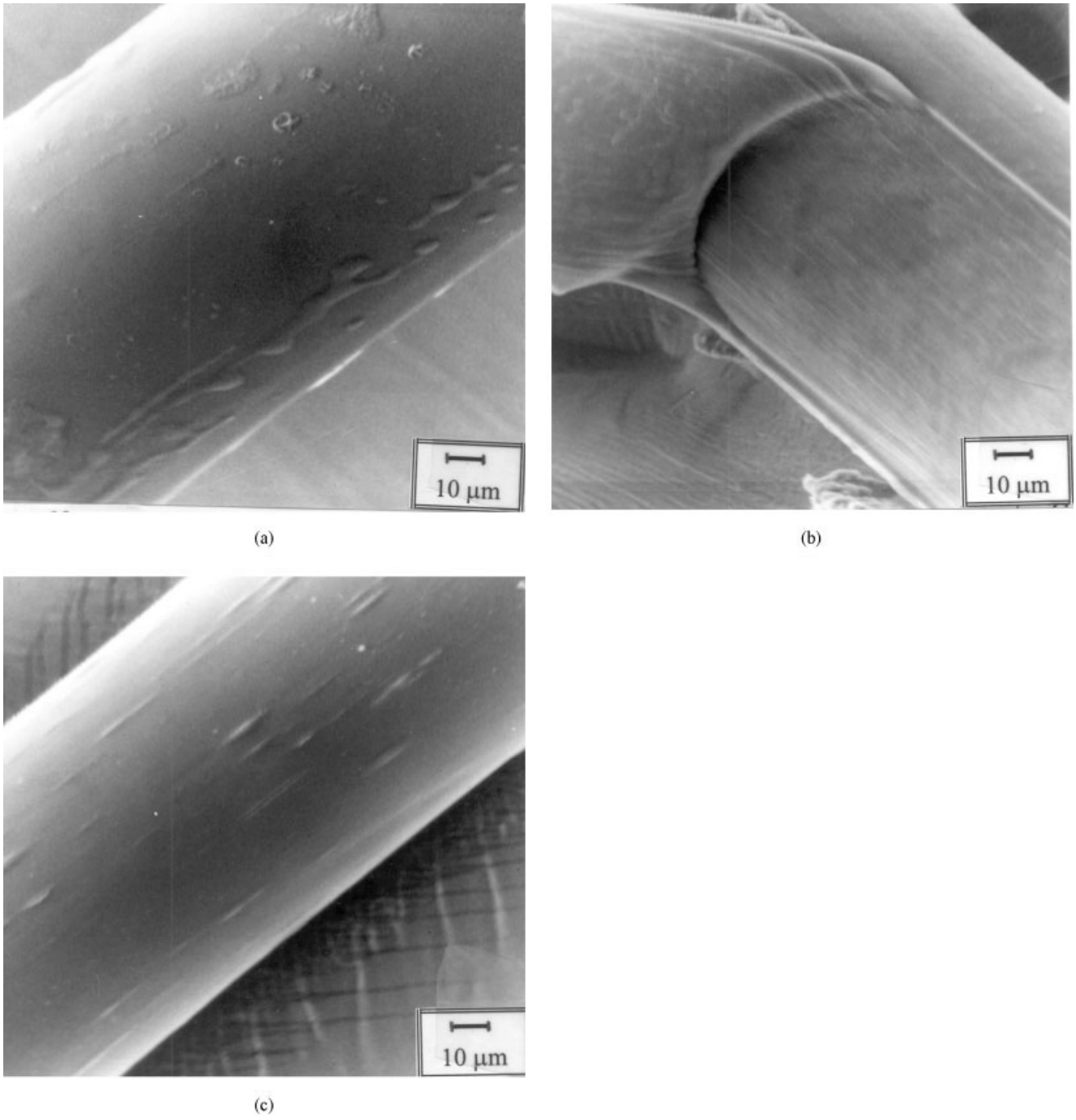

Figure 9 Electron micrographs of (a) the surface (b) an inner structure revealed by splitting, and (c) an inner structure revealed by chromic acid etching of continuously drawn fiber, spun from the 100/0 fiber/molding grade polymer blend.

of low lateral cohesion of the highly developed fibrillar structure seen in Figure 10(b). After 100 h chromic acid etching at room temperature, a part of the fiber was etched, because of its highly voided structure and platelets of acid resistant structure remained (Fig. 10(c)). For these etching-resistant harder regions, parallel developed in longitudinal section with periodic regularity is suggested to be the location of residual molecular entanglements.[47]

Molecular and crystal orientation

The average molecular orientation was determined by the birefringence measurements and from the sonic-velocity method. An excellent agreement between the values obtained by both methods was achieved, the difference in the absolute values being less than 5%. For the determination of amorphous orientation, the average molecular orientation obtained by sonic-

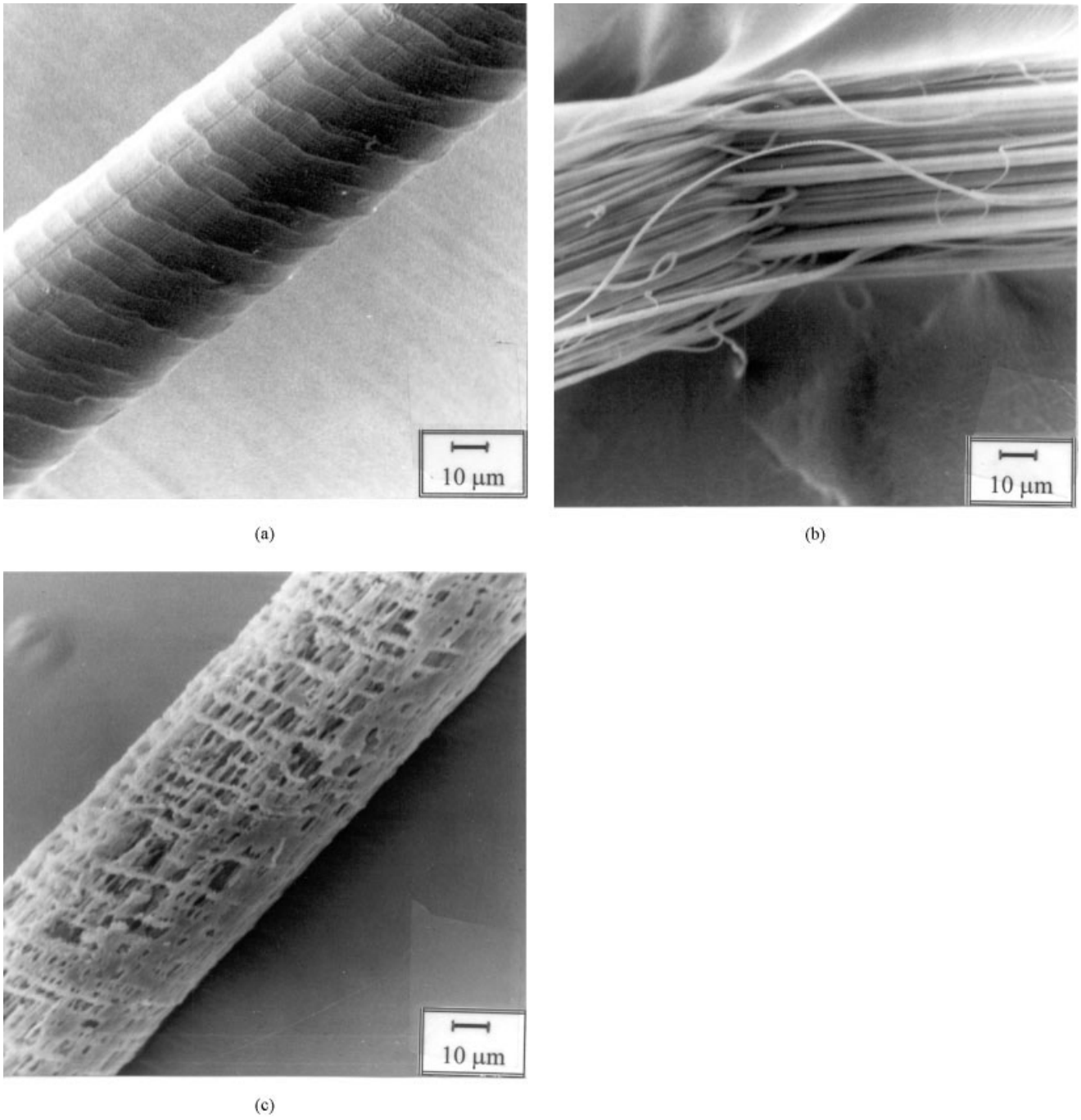

Figure 10 Electron micrographs of (a) the surface (b) an inner structure revealed by splitting, and (c) an inner structure revealed by chromic acid etching of discontinuously drawn fiber, spun from the 100/0 fiber/molding grade polymer blend.

velocity method was used. The level of amorphous orientation was calculated from the following equation

$$\frac{3}{2}(E_u^{-1} - E_d^{-1}) = \frac{x_c f_c}{E_{t,c}^0} + \frac{(1 - x_c) f_{\text{am}}}{E_{t,\text{am}}^0} \tag{4}$$

where E_u is the sonic modulus of unoriented sample, E_d measured sonic modulus of fiber, $E_{t,c}^0$ intrinsic lateral modulus of the crystal and $E_{t,\text{am}}^0$ intrinsic sonic modulus of the amorphous region, x_c crystallinity index, and f_c crystalline orientation. The crystalline orientation function, given as Herman-Stein factor

$$f_c = \frac{3\langle \cos^2 \phi_{c,Z} \rangle - 1}{2} \tag{5}$$

where $\langle \cos^2 \phi_{c,Z} \rangle$ is the mean-square cosine of the angle between the fiber axes and *c*-crystallographic axis, was

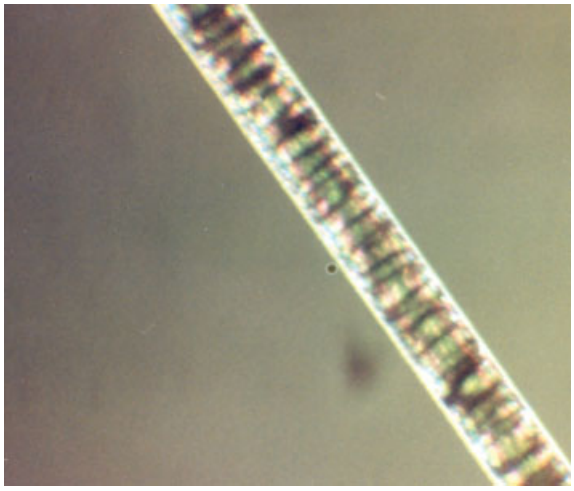

Figure 11 Optical micrograph of discontinuously drawn fiber, spun from the 100/0 fiber/molding grade polymer blend. [Color figure can be viewed in the online issue, which is available at www.interscience.wiley.com.]

calculated from the (110) and (040) reflections by the following relation

$$\langle \cos^2 \phi_{c,Z} \rangle = 1 - 1.099 \langle \cos^2 \phi_{110,Z} \rangle - 0.901 \langle \cos^2 \phi_{040,Z} \rangle \quad (6)$$

Figure 12 shows that differences exist between the structural characteristics of the continuously drawn fibers and the discontinuously drawn fibers, regarding molecular orientation. The average orientation function, as well as the crystalline and amorphous orientation functions increased with additional hot drawing of fibers. The orientation function of the crystallite axis *c* is higher at highly drawn fibers in comparison with the continuously drawn fibers. Even much higher difference between the continuously drawn fibers and discontinuously drawn fibers was noted for the orientation function of amorphous chains, i.e., around 30% higher values were obtained for the discontinuously drawn fibers. As seen from Figure 12, no influence of the blend composition on the crystalline orientation function could be observed. The difference between continuously drawn fibers as well as the difference between discontinuously drawn fibers spun from different blend compositions is in the range of the value's statistical deviation. On the other hand, some influence of the blend composition could be observed at the amorphous orientation function. A slight increase with increasing the content of the molding-grade polymer in the blend at the continuously drawn fibers is observed, while at discontinuously drawn fibers a decreasing tendency is noted.

Correlation between mechanical properties, crystallinity and orientation

It is well known that the crystallinity, the size of crystallites, and their orientation have basic influence on the mechanical properties of drawn fibers.[11,36,48,49] In Figures 13–15, the tensile strength (Fig. 13), the elastic modulus (Fig. 14) and dynamic modulus (Fig. 15) are shown as a function of the crystallinity index. From Figure 13 it is clearly seen that the tensile strength increases with the crystallinity determined by

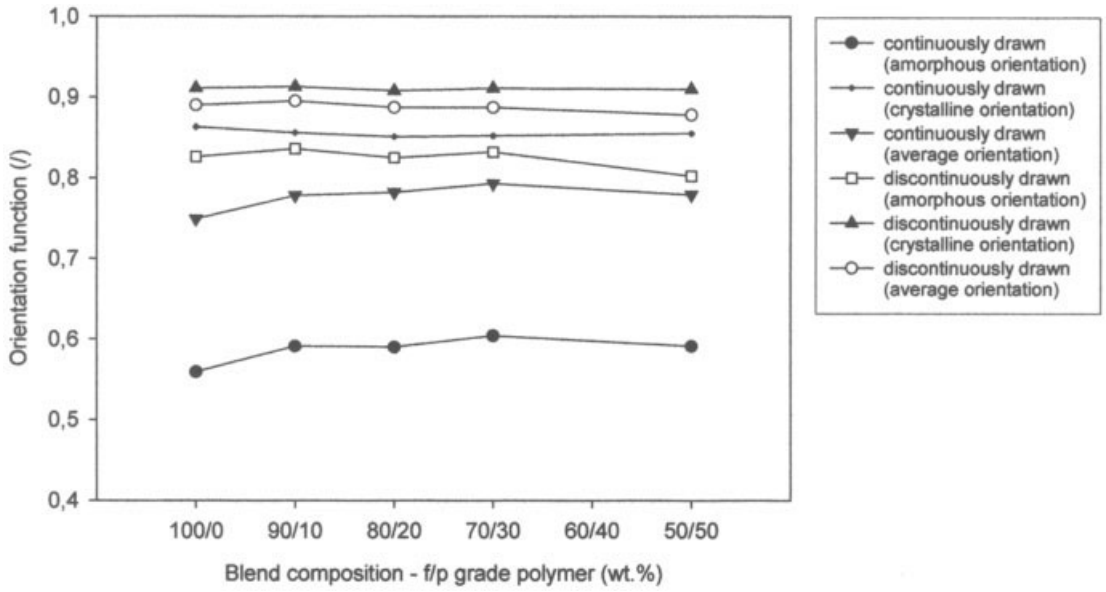

Figure 12 Average molecular orientation function (f_{av}), crystalline orientation function (f_c), and amorphous orientation function (f_{am}) of the continuously and discontinuously drawn fibers, spun from the 100/0, 90/10, 80/20, 70/30, and 50/50 fiber/molding grade polymer blend.

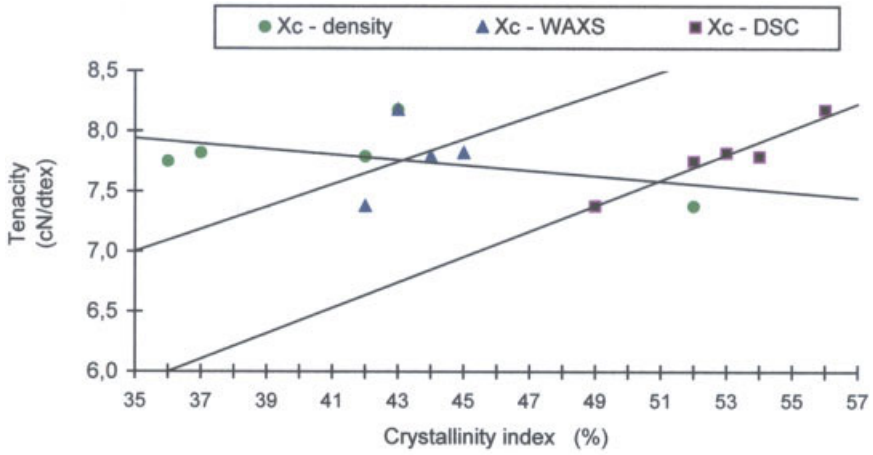

Figure 13 Tensile strength of discontinuously drawn fibers as a function of crystallinity. [Color figure can be viewed in the online issue, which is available at www.interscience.wiley.com.]

the WAXS and DSC methods and decreases with the crystallinity determined from the density measurements. Similar results were obtained for the elastic modulus (Fig. 14) and dynamic modulus (Fig. 15); increasing tendency with the crystallinity determined by the WAXS and DSC methods and a decreasing

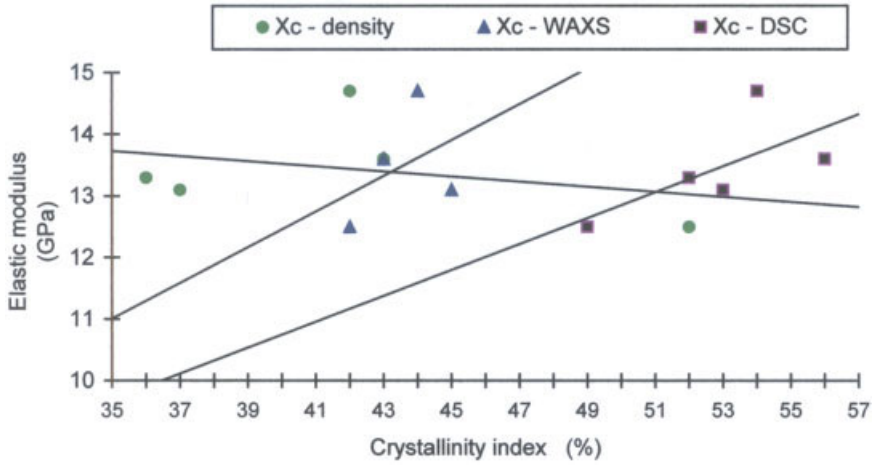

Figure 14 Elastic modulus of discontinuously drawn fibers as a function of crystallinity. [Color figure can be viewed in the online issue, which is available at www.interscience.wiley.com.]

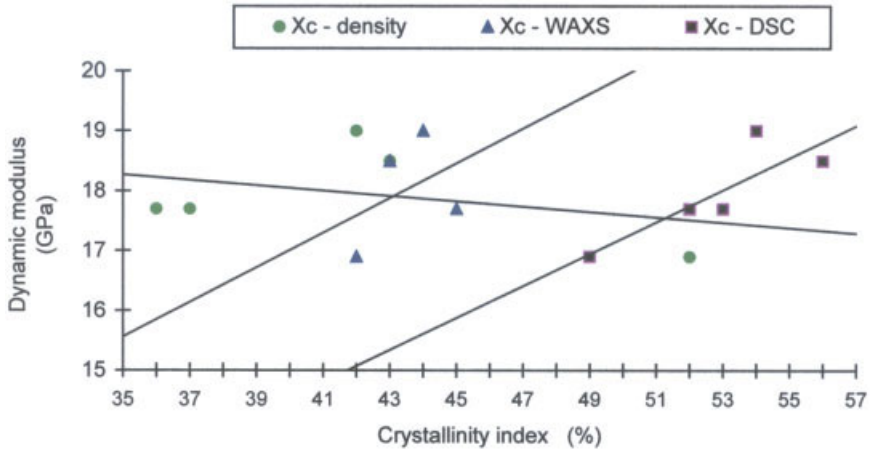

Figure 15 Dynamic modulus of discontinuously drawn fibers as a function of crystallinity. [Color figure can be viewed in the online issue, which is available at www.interscience.wiley.com.]

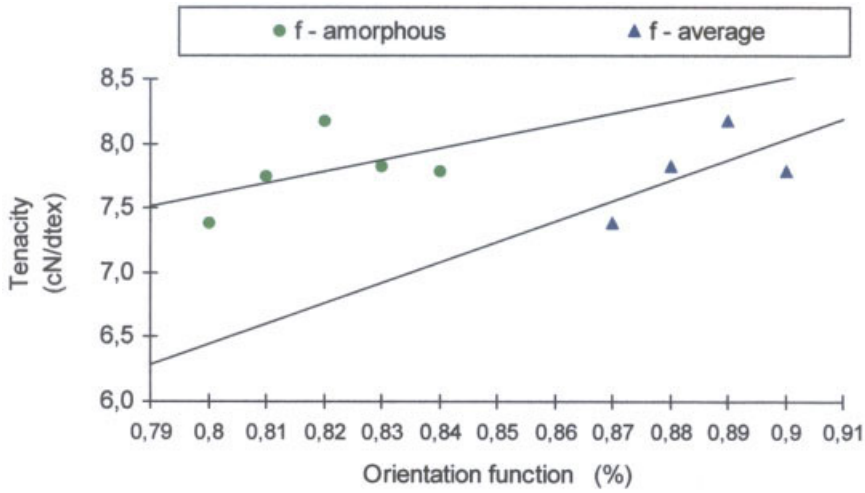

Figure 16 Tensile strength of discontinuously drawn fibers as a function of average and amorphous molecular orientation function. [Color figure can be viewed in the online issue, which is available at www.interscience.wiley.com.]

tendency with the crystallinity determined from the density data. The tensile strength and both moduli as a function of the crystallinity index have a linear character, although the values deviate in some cases and the correlation being rather low.

The mechanical properties of drawn fibers, besides depending on the crystallinity and number of taut tie molecules, also depends on the orientation of the macromolecules in the crystalline and amorphous domains. In Figures 16–18, the mechanical properties of the discontinuously drawn fibers are plotted against the orientation functions. It is clearly seen that the tensile strength, the elastic, and dynamic moduli increase with molecular orientation. Linear dependence is seen in the case of tensile strength (Fig. 16) and both moduli (Figs. 17 and 18), correlation factor being of the order of 0.73 for tensile strength, 0.95 for the static elastic modulus and 0.97 for the dynamic modulus. Because all discontinuously drawn fibers exhibit similar high values of crystalline orientation function, a low correlation with the mechanical properties was determined. Quite different results were obtained for the amorphous orientation function, where the mechanical properties of fibers investigated in our study have shown a good agreement with the amorphous orientation, the correlation factor being, in all cases, higher than 0.8.

CONCLUSIONS

The following conclusions can be drawn:

1. Melt spinning of binary PP blends of different molecular weights on a laboratory spin-draw device, with immediate moderate and subsequent

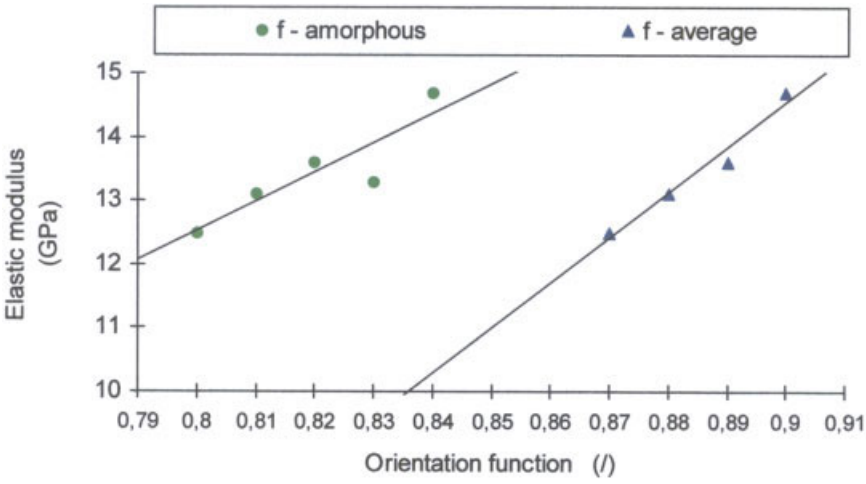

Figure 17 Elastic modulus of discontinuously drawn fibers as a function of average and amorphous molecular orientation function. [Color figure can be viewed in the online issue, which is available at www.interscience.wiley.com.]

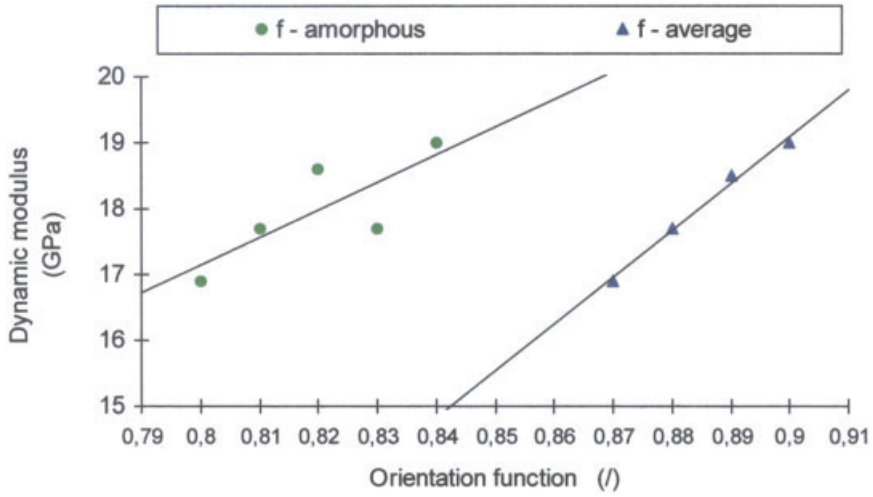

Figure 18 Dynamic modulus of discontinuously drawn fibers as a function of average and amorphous molecular orientation function. [Color figure can be viewed in the online issue, which is available at www.interscience.wiley.com.]

severe hot drawing, enables the production of fibers with improved mechanical properties, under industrially feasible conditions.

2. Moderate in-line drawing of as-spun filaments at 50°C causes the development of so-called oriented "smectic" structure.
3. Additional drawing to the limiting draw ratio at the temperature of 145°C results in a well-oriented fibrillar structure, with only *c*-axis oriented monoclinic crystalline modification present. The structural changes are accompanied by increased orientation of both crystalline and amorphous domains, increased crystallinity, and development of a highly voided structure.
4. Some influence of polymer blend composition on the structure of drawn fibers was noted too. At continuously moderately drawn fibers, the blend composition had no effect on the size of crystallites and long period, whereas the crystallinity, as well as amorphous orientation increased with increasing the content of the molding-grade polymer in the blend. At discontinuously drawn fibers, increasing the content of the molding-grade polymer in the blend resulted in lowering the maximum attainable draw ratio and consequently in decreasing the size of crystalline and amorphous domains, density and crystallinity, as well as amorphous orientation.
5. The results of this study confirm that the thermodynamically unstable oriented "smectic" structure is a suitable precursor for the production of high-tenacity, high-modulus PP fibers and that by blending the fiber-grade CR-polymer by a small percentage of the molding-grade polymer maximization of elastic modulus is achieved, mainly because of higher orientation of crystalline and amorphous domains.

The author is greatly indebted to Prof. Dr. S. Malej-Kveder for having initiated and supervised this work. The author thanks the Institute of Physical Chemistry at University of Graz for the WAXS and SAXS facilities. The author also thanks Prof. Dr. P. Zipper for his help with the X-ray diffractometry.

References

1. Gregor-Svetec, D. Tekstilec 2000, 43, 387.
2. Zahn, H. Lenziger Berichte 1986, 60, 7.
3. Spruiell, J. E.; White, J. L. Appl Polym Symp 1975, 27, 121.
4. Keller, A.; Machin, M. J. J Macromol Sci B 1967, 1, 41.
5. Tucker, P.; George, W. Polym Eng Sci 1972, 12, 364.
6. Norton, D. R.; Keller, A. Polymer 1985, 26, 704.
7. Clark, E. S.; Spruiell, J. E. Polym Eng Sci 1976, 16, 176.
8. Lu, F.; Spruiell, J. E. J Appl Polym Sci 1987, 34, 1521.
9. Minoshima, W.; White, J. L.; Spruiell, J. E. J Appl Polym Sci 1980, 25, 287.
10. Parrini, P. Makromol Chem 1963, 62, 83.
11. Ahmed, M. Textile Science and Technology, Vol. 5, Polypropylene Fibers—Science and Technology; Elsevier: Amsterdam, 1982.
12. Compostella, M. Angew Chem 1962, 74, 618.
13. Misra, S.; Spruiell, J. E.; Richeson, G. C. J Appl Polym Sci 1995, 56, 1761.
14. Andreassen, E.; Myhre, O. J.; Hinrichsen, E. L.; Grostad, K. J Appl Polym Sci 1994, 52, 1505.
15. Nogales, A.; Hsiao, B. S.; Somani, R. H.; Srinivas, S.; Tsou, A. H.; Balta-Calleja, F. J.; Ezquerra, T. A. Polymer 2001, 42, 5247.
16. Samuels, R. J. J Macromol Sci Phys B 1970, 4, 701.
17. Samuels, R. J. Polym Eng Sci 1976, 16, 327.
18. Peterlin, A. J Polym Eng Sci 1974, 14, 627.
19. Peterlin, A. Colloid Polym Sci 1987, 265, 357.
20. Taylor, W. N.; Clark, E. S. Polym Eng Sci 1978, 18, 518.
21. Spruiell, J. E. In Structure Formation in Polymeric Fibers; Salem, D. R., Ed.; Hanser: Munich, 2001.
22. Koike, Y.; Cakmak, M. Polymer 2003, 44, 4249.
23. Hautojärvi, J.; Niemi, H. Textil Res J 2000, 70, 820.
24. Broda, J. Polymer 2003, 44, 1619.
25. Risnes, O.; Mather, R. R.; Neville, A. Polymer 2003, 44, 89.
26. Gregor-Svetec, D.; Sluga, F. J Appl Polym Sci 2005, 98, 1.

27. Weidinger, A.; Hermans, P. H. Makromol Chem 1961, 50, 98.
28. Klug, H. P.; Alexander, L. E. X-ray Diffraction Procedures; Wiley: New York, 1973.
29. Wilchinsky, Z. W. J Appl Phys 1960, 31, 1969.
30. Wenig, W.; Brämer, R. Colloid Polym Sci 1978, 256, 125.
31. Brämer, R. Colloid Polym Sci 1974, 252, 504.
32. Porod, G. In Small Angle X-ray Scattering; Glatter, O., Kratky, O. Eds.; Academic Press: London, 1982.
33. Jánosi, A. Z Phys B: Condens Matter 1986, 63, 375.
34. Juilfs, J. Melliand Textilberichte 1959, 40, 963.
35. Stein, R. S. J Polym Sci 1958, 31, 327.
36. Samuels, R. J. Structured Polymer Properties; Wiley: New York, 1974.
37. Natta, G.; Corradini, P. Nuovo Cimento Suppl 1960, 15, 40.
38. Hosemann, R.; Wilke, W. Makromol Chem 1968, 118, 230.
39. Gailey, J. A.; Ralston, P. H. Soc Plast Eng Trans 1964, 4, 29.
40. Gezowich, D. M.; Geil, P. H. Polym Eng Sci 1968, 8, 202.
41. Bodor, G.; Grell, M.; Kallo, A. Faserforsch Textil Tech 1964, 15, 527.
42. Farrow, G. J Appl Polym Sci 1965, 9, 1227.
43. Caldas, V.; Brown, G. R.; Nohr, R. S.; MacDonald, J. G.; Raboin, L. E. Polymer 1994, 35, 899.
44. Ferrero, A.; Ferracini, E.; Mazzavillani, A.; Malta, V. J Macromol Sci B Phys 2000, 39, 109.
45. Wang, Z.-G.; Hsiao, B. S.; Srinivas, S.; Brown, G. M.; Tsou, A. H.; Cheng, S. Z. D.; Stein, R. S. Polymer 2001, 42, 7561.
46. Garton, A.; Carlsson, D. J.; Sturgeon, P. Z.; Wiles, D. M. J Polym Sci Polym Phys Ed 1977, 15, 2013.
47. Amornsakchai, T.; Olley, R. H.; Bassett, D. C.; Al-Hussein, M. O. M.; Unwin, A. P. M.; Ward, I. M. Polymer 2000, 41, 8291.
48. Peterlin, A. Colloid Polym Sci 1975, 253, 809.
49. Kitao, T.; Spruiell, J. E.; White, J. L. Polym Eng Sci 1979, 19, 761.